energies

MDPI

Article

Passivity-Based Control of Dual Active Bridge Converter in Constant Power Load Condition

Jianguo Li [1,*], Yuming Zhao [2], Xuezhi Wu [3], Yajing Zhang [1] and Jiuhe Wang [1]

[1] School of Automation, Beijing Information Science and Technology University, Beijing 100192, China
[2] Shenzhen Power Supply Corporation, Shenzhen 518048, China
[3] National Active Distribution Network Technology Research Center, Beijing Jiaotong University, Beijing 100044, China
* Correspondence: lijianguo@bistu.edu.cn

Abstract: This paper presents a passivity-based control (PBC) based on the Euler–Lagrange (EL) model for dual active bridge (DAB) converters in the constant power load (CPL) condition. The EL model, which is derived from Kirchhoff's current equations at the input and output nodes, is first presented in the DAB application, and the bidirectional CPL is considered in the theoretical analysis, simulation, and physical verification. The PBC has strong robustness to large-signal disturbance and negative incremental resistance load, and it is suitable for DAB converters in the CPL condition. In this paper, the DAB's EL model, passivity analysis, stability analysis, and controller design are described in detail. The simulation results based on SIMULINK are also given in this paper. Finally, a DAB converter prototype is built to demonstrate the validity and feasibility of the proposed approach.

Keywords: dual active bridge; passivity-based control; constant power load

Citation: Li, J.; Zhao, Y.; Wu, X.; Zhang, Y.; Wang, J. Passivity-Based Control of Dual Active Bridge Converter in Constant Power Load Condition. *Energies* **2022**, *15*, 6685. https://doi.org/10.3390/en15186685

Academic Editors: Yizhen Wang, Yu Wang and Biyun Chen

Received: 23 August 2022
Accepted: 12 September 2022
Published: 13 September 2022

1. Introduction

In 1991, the dual active bridge (DAB) was proposed by R.W. De Doncker. It has the advantages of soft-switching, bidirectional power flow capabilities, buck–boost operation, galvanic isolation, high power density, and a high degree of modularization [1,2].

Thereafter, DABs gained increasing attention and practical application in low DC voltage and even in medium DC voltage when several DABs are series-connected to achieve higher voltage access [3–5]. DABs are the key component in DC distribution applications.

Normally, the power is transmitted by voltage stabilizing control or constant power control. The pulse modulation of fixing the primary side and lagging or leading the commutation of the secondary side according to the power direction is adopted [6].

Whether in constant power control or voltage stabilizing control with tight regulation, the load behaves as a constant power load (CPL) within its control-loop bandwidth. Its negative incremental resistance characteristic is generally the origin of the converter instability [7,8].

Some closed-loop regulations should be adopted to ensure the DAB's stable operation and fast perturbation rejection. A novel Lyapunov-function-based control [9] and state-observer-based PI-PBC control [10,11] are presented to guarantee the converter's global asymptotic stability. The full-order continuous-time average modeling of DABs was studied in [12]. The linear control, which is based on the small-signal model, is most popular in a DAB's closed-loop control, and it mainly includes pole-placement control and PI control. However, pole-placement control has its disadvantages, such as its complexity and difficult implementation [13,14]. Although the proportional–integral (PI) control is simple and easy to implement, it suffers from the drawback of inconsistent performance across the entire operating range [15].

Some non-linear controls are also employed, including feedback linearization control, flatness-based control [16–18], model predictive control [19,20], sliding mode control [21,22],

and virtual power control [23]. Although these non-linear controls can give high performance, they are complex and difficult to make ready for physical application.

The passivity-based control (PBC) is the most practical non-linear control technique due to its simplicity and easy implementation [24]. The PBC reshapes the dissipated energy from the system's Euler–Lagrange representation and then injects a virtual resistance matrix to dampen the system and ensure its passivity [25]. Once every converter is guaranteed to be passive and stable, their interconnected or cascaded system is also passive and stable, so it is used in the power conversion system [26], rectifier [27,28], PV [29,30], STATCOM [31], and other converters [32,33].

In [34], the port-controlled phasor Hamiltonian (PCPH) model of DABs was proposed for the first time, but it is only valid for low-power applications because of its sinusoidal pulse width modulation, and it is only verified by Opal-RT and dSPACE simulators. Moreover, based on the PCPH model, [35] applied Interconnection and Damping Assignment PBC (IDA-PBC) to a DAB's controller design; the hardware-in-loop (HIL) experiments and low-power prototype experiments were all performed in large-signal disturbance, but only resistive load was used in the verification, and the power flowed only from the primary to the secondary side. Although the CPL is considered in DAB-based shipboard power systems, it is only verified by simulation, and it needs further physical experimental verification [36].

In this study, the PBC based on the Euler–Lagrange (EL) model is applied to a DAB's application for the first time, and the bi-directional CPL is considered in SIMULINK simulation as well as in physical experiments.

The rest is organized as follows. In Section 2, the DAB modeling in EL form is presented. Section 3 implements passivity analysis, stability analysis, and controller design sequentially. Later, in Sections 4 and 5, respectively, the SIMULINK simulation and prototype implementation are described with results. Finally, Section 6 states the conclusion.

2. Topology Analysis

The DAB is made up of S_1–S_8, L_1, T, C_1, and C_2, as depicted in Figure 1. S_1–S_8 are fully controlled power switches, such as MOSFET, IGBT, IGCT, et al.; S_1-S_4 make up the primary bridge converter; S_5–S_8 make up the secondary bridge converter; L_1 is an inductor for energy exchange; T is a high-frequency (HF) transformer for voltage matching and electrical isolation; C_1 and C_2 are capacitors for primary and secondary filtering and energy exchange; and R_1 and R_2 are equivalent resistances to simulate primary and secondary power losses. A DAB converter can realize voltage conversion between different voltages with electrical isolation, and it can realize bidirectional power exchange at the same time.

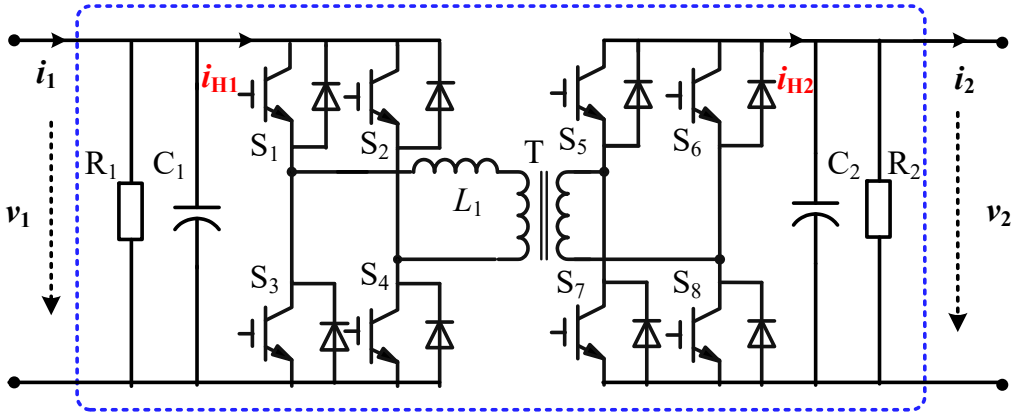

Figure 1. The DAB topology.

According to the related research [2], the power transmitted by the DAB can be expressed as

$$P = \frac{Nv_1v_2}{2f_sL_1}D(1-|D|), \tag{1}$$

where N is the HF transformer's turn ratio; v_1 and v_2 are the primary voltage and secondary voltage, respectively; f_s is the switching frequency of the switches; and D is the phase shift duty ratio, which means that the phase shift time is equal to $DT_s/2$, where $T_s = 1/f_s$ is the switching period.

It is assumed that the converter's loss can be ignored, and the primary average bridge current and the secondary average bridge current can be described as

$$\begin{cases} i_{H1} = \frac{P}{v_1} = \frac{Nv_2}{2f_sL_1}D(1-|D|) = K\frac{v_2}{\omega_sL_1}, \\ i_{H2} = \frac{P}{v_2} = \frac{Nv_1}{2f_sL_1}D(1-|D|) = K\frac{v_1}{\omega_sL_1}, \end{cases} \tag{2}$$

where

$$K = N\pi D(1-|D|). \tag{3}$$

According to Kirchhoff's current law, we can further obtain the formula

$$\begin{cases} C_1\frac{dv_1}{dt} + \frac{1}{R_1}v_1 + \frac{K}{\omega_sL_1}v_2 = i_1, \\ C_2\frac{dv_2}{dt} + \frac{1}{R_2}v_2 - \frac{K}{\omega_sL_1}v_1 = -i_2. \end{cases} \tag{4}$$

where i_1 and i_2 are the input and output currents of the DAB converter, respectively. Assuming the resistors, capacitors, and inductors are all time-invariant, the controller can be designed based on these differential equations, and its properties can also be exploited in the closed-loop system analysis.

If $\boldsymbol{X} = (v_1, v_2)^T$ and $\boldsymbol{V} = (i_1, -i_2)^T$ are selected as state variables and input variables, respectively, (4) can be expressed as a standard Euler equation in the form of

$$\boldsymbol{M}\dot{\boldsymbol{X}} + \boldsymbol{J}\boldsymbol{X} + \boldsymbol{R}\boldsymbol{X} = \boldsymbol{V}, \tag{5}$$

where $\boldsymbol{M}$ is a positive definite symmetric coefficient matrix, i.e., $\boldsymbol{M}^T = \boldsymbol{M} > 0$. $\boldsymbol{J}$ is a skew-symmetric coefficient matrix, i.e., $\boldsymbol{J}^T = -\boldsymbol{J}$. $\boldsymbol{R}$ is a positive coefficient matrix, i.e., $\boldsymbol{R}^T = \boldsymbol{R} > 0$, which means that the converter has a dissipative characteristic.

$$\boldsymbol{M} = \begin{pmatrix} C_1 & 0 \\ 0 & C_2 \end{pmatrix}, \boldsymbol{J} = \begin{pmatrix} 0 & \frac{K}{\omega_sL_1} \\ -\frac{K}{\omega_sL_1} & 0 \end{pmatrix}, \boldsymbol{R} = \begin{pmatrix} 1/R_1 & 0 \\ 0 & 1/R_2 \end{pmatrix} \tag{6}$$

3. PBC Controller Design

3.1. Passivity Analysis

It is assumed that the energy storage function is

$$\boldsymbol{H} = \frac{1}{2}\boldsymbol{X}^T\boldsymbol{M}\boldsymbol{X} = \frac{1}{2}(C_1{v_1}^2 + C_2{v_2}^2) \geq 0, \tag{7}$$

and the change rate of energy storage function can be obtained as

$$\begin{aligned} \dot{\boldsymbol{H}} &= \boldsymbol{X}^T\boldsymbol{M}\dot{\boldsymbol{X}} = \boldsymbol{X}^T(\boldsymbol{V} - \boldsymbol{J}\boldsymbol{X} - \boldsymbol{R}\boldsymbol{X}) = \boldsymbol{X}^T\boldsymbol{V} - \boldsymbol{X}^T\boldsymbol{R}\boldsymbol{X} \\ &= v_1i_1 - v_2i_2 - ({v_1}^2/R_1 + {v_2}^2/R_2). \end{aligned} \tag{8}$$

For all input variables $\boldsymbol{V}$, if the output variable is selected as $\boldsymbol{Y} = \boldsymbol{X}$, and the function $\boldsymbol{Q}(\boldsymbol{X})$ is defined as ${v_1}^2/R_1 + {v_2}^2/R_2$, then (8) can be further rewritten as

$$\dot{\boldsymbol{H}} \leq \boldsymbol{Y}^T\boldsymbol{V} - \boldsymbol{Q}(\boldsymbol{X}), \tag{9}$$

where $\boldsymbol{Q}(\boldsymbol{X})$ is a positive definite function. According to passivity theory, the DAB converter is strictly passive.

3.2. Stability Analysis

It is assumed that the reference value is $\boldsymbol{X}^* = (v_1^* \; v_2^*)^{\mathrm{T}}$, the error vector is $\boldsymbol{X}_{\mathrm{e}} = \boldsymbol{X} - \boldsymbol{X}^*$, and (5) can be further expressed in $\boldsymbol{X}_{\mathrm{e}}$ form as

$$\boldsymbol{M}\dot{\boldsymbol{X}}_{\mathrm{e}} + \boldsymbol{R}\boldsymbol{X}_{\mathrm{e}} = \boldsymbol{M}\dot{\boldsymbol{X}} - \boldsymbol{M}\dot{\boldsymbol{X}}* + \boldsymbol{R}(\boldsymbol{X} - \boldsymbol{X}*) = \boldsymbol{V} - (\boldsymbol{M}\dot{\boldsymbol{X}}* + \boldsymbol{J}\boldsymbol{X} + \boldsymbol{R}\boldsymbol{X}*), \tag{10}$$

Obviously, when $\boldsymbol{X}$ approaches $\boldsymbol{X}^*$, $\boldsymbol{X}_{\mathrm{e}}$ will approach 0, and Equation (10) will be equal to 0, that is

$$\boldsymbol{M}\dot{\boldsymbol{X}}_{\mathrm{e}} + \boldsymbol{R}\boldsymbol{X}_{\mathrm{e}} = \boldsymbol{V} - (\boldsymbol{M}\dot{\boldsymbol{X}}* + \boldsymbol{J}\boldsymbol{X} + \boldsymbol{R}\boldsymbol{X}*) = 0, \tag{11}$$

On the other hand, according to (8), the change rate of storage energy function expressed in $\boldsymbol{X}_{\mathrm{e}}$ form is

$$\dot{\boldsymbol{H}}_{\mathrm{e}} = \boldsymbol{X}_{\mathrm{e}}{}^{\mathrm{T}}\boldsymbol{M}\dot{\boldsymbol{X}}_{\mathrm{e}} = -\boldsymbol{X}_{\mathrm{e}}{}^{\mathrm{T}}\boldsymbol{R}\boldsymbol{X}_{\mathrm{e}} \leq 0. \tag{12}$$

Therefore, the value of $\mathrm{d}\boldsymbol{H}_{\mathrm{e}}(\boldsymbol{X}_{\mathrm{e}})/\mathrm{d}t$ is not always 0 for any initial state $\boldsymbol{X}_{\mathrm{e}} \neq 0$, and when $||\boldsymbol{X}_{\mathrm{e}}|| \to \infty$, there is $\boldsymbol{H}_{\mathrm{e}}(\boldsymbol{X}_{\mathrm{e}}) \to \infty$. Consequently, the designed PBC controller can realize the asymptotic stability of the DAB converter.

3.3. Controller Design

According to (11), the PBC controller can be designed as

$$\boldsymbol{V} = \boldsymbol{M}\dot{\boldsymbol{X}}* + \boldsymbol{J}\boldsymbol{X} + \boldsymbol{R}\boldsymbol{X}*, \tag{13}$$

To accelerate $\boldsymbol{X}_{\mathrm{e}}$ convergence to 0, a damping injection matrix is used, and (13) further becomes

$$\boldsymbol{V} = \boldsymbol{M}\dot{\boldsymbol{X}}* + \boldsymbol{J}\boldsymbol{X} + \boldsymbol{R}\boldsymbol{X}* - \boldsymbol{R}_{\mathrm{d}}\boldsymbol{X}_{\mathrm{e}}, \tag{14}$$

where $\boldsymbol{R}_{\mathrm{d}} = \mathrm{diag}\{\mathrm{g}_{11}, \mathrm{g}_{22}\}$ is the damping injection matrix.

That is

$$\begin{cases} i_1 = C_1\frac{\mathrm{d}v_1*}{\mathrm{d}t} + \frac{K}{\omega_{\mathrm{s}}L_1}v_2 + \frac{1}{R_1}v_1* - \mathrm{g}_{11}(v_1 - v_1*), \\ -i_2 = C_2\frac{\mathrm{d}v_2*}{\mathrm{d}t} - \frac{K}{\omega_{\mathrm{s}}L_1}v_1 + \frac{1}{R_2}v_2* - \mathrm{g}_{22}(v_2 - v_2*). \end{cases} \tag{15}$$

When the DAB works in constant secondary voltage (CSV) mode, the control target value is reference v_2^*, and (15) can be simplified to

$$K = \frac{\omega_{\mathrm{s}}L_1[i_2 + C_2\frac{\mathrm{d}v_2*}{\mathrm{d}t} + \frac{1}{R_2}v_2* - \mathrm{g}_{22}(v_2 - v_2*)]}{v_1}. \tag{16}$$

When the DAB works in constant primary voltage (CPV) mode, the control target value is reference v_1^*, and (15) can be further simplified to

$$K = \frac{\omega_{\mathrm{s}}L_1[i_1 - C_1\frac{\mathrm{d}v_1*}{\mathrm{d}t} - \frac{1}{R_1}v_1* + \mathrm{g}_{11}(v_1 - v_1*)]}{v_2}. \tag{17}$$

Whether in CSV or CPV mode, the variable K can be calculated from (16) or (17). Then, D can be obtained by solving the monadic quadratic Equation (3).

When K is greater than 0, D is also greater than 0, which means that the power is transmitted from the primary side to the secondary side, so we can obtain

$$0 < D = \frac{1}{2} - \sqrt{\frac{1}{4} - \frac{K}{N\pi}} < \frac{1}{2}, \text{ when } K \geq 0. \tag{18}$$

When K is less than 0, D is also less than 0, which means that the power is transmitted from the secondary to the primary side, so we can obtain

$$-\frac{1}{2} < D = -\frac{1}{2} + \sqrt{\frac{1}{4} + \frac{K}{N\pi}} < 0, \text{ when } K < 0. \tag{19}$$

According to the analysis above, (16) or (17) is used to calculate the variable K in CSV and CPV mode, respectively. Then (18) or (19) is used to calculate the phase shift duty ratio according to the power direction. The PBC control diagram is shown in Figure 2.

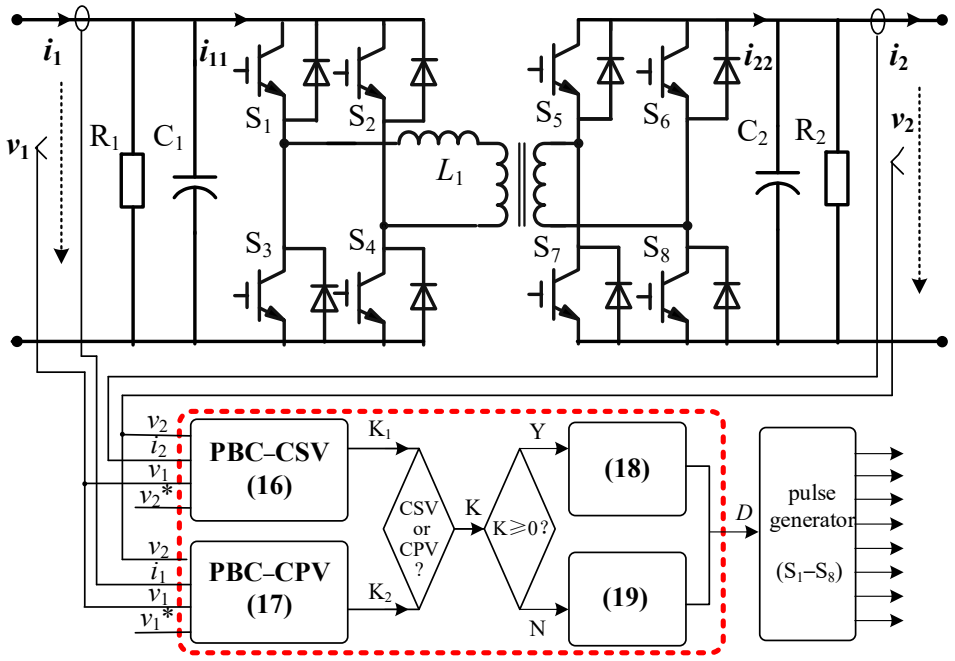

Figure 2. The PBC control diagram of the DAB converter.

3.4. Closed-Loop System Stability Analysis

Substituting the control (15) into the system model (4), the closed-loop system can be written as

$$\begin{cases} C_1 \frac{d}{dt} x_{e1} = -\frac{1}{R_1} x_{e1} - g_{11} x_{e1} \\ C_2 \frac{d}{dt} x_{e2} = -\frac{1}{R_2} x_{e2} - g_{22} x_{e2} \end{cases} \tag{20}$$

where $x_{e1} = v_1 - v_1{}^*$, $x_{e2} = v_2 - v_2{}^*$. We can select the Lyapunov function as

$$\mathbf{W}(x_{e1}, x_{e2}) = \frac{1}{2} C_1 {x_{e1}}^2 + \frac{1}{2} C_2 {x_{e2}}^2 \geq 0 \tag{21}$$

The time derivative of $\mathbf{W}(x_{e1}, x_{e2})$ along the closed-loop system trajectory (20) is shown as

$$\begin{aligned} \dot{\mathbf{W}}(x_{e1}, x_{e2}) &= (-\tfrac{1}{R_1} x_{e1} - g_{11} x_{e1}) x_{e1} + (-\tfrac{1}{R_2} x_{e2} - g_{22} x_{e2}) x_{e2} \\ &= -(\tfrac{1}{R_1} + g_{11}) {x_{e1}}^2 - (\tfrac{1}{R_2} + g_{22}) {x_{e2}}^2 \leq 0 \end{aligned} \tag{22}$$

Since Equation (21) is positive definite and Equation (22) is negative definite, the equilibrium state of the closed-loop system at the state space origin $\boldsymbol{X}_e = (x_{e1}, x_{e2})^T = \mathbf{0} \in \mathbf{R}^2$ is asymptotically stable. Moreover, when $||\boldsymbol{X}_e|| \to \infty$, $\mathbf{W}(\boldsymbol{X}_e) \to \infty$ is satisfied for any $t \geq 0$. Therefore, according to the Lyapunov stability theorem, the closed-loop system is asymptotically stable in a large range of the equilibrium state.

4. Simulation

To validate the effectiveness of PBC based on the EL model for a DAB converter in the CPL condition, time-domain simulations are carried out in SIMULINK under voltage and power perturbation. The main parameters are listed in Table 1.

Table 1. Main parameters of DAB converter.

	Parameters	Value
1	DC voltage v_1 (V)	750
2	capacitance C_1 (μF)	2200
3	resistance R_1 (Ω)	100×10^3
4	voltage v_2 (V)	375
5	capacitance C_2 (μF)	2200
6	resistance R_2 (Ω)	100×10^3
7	inductance L_1 (μH)	200
8	HF transformer's turn ratio	750:375
9	DAB switching frequency (kHz)	10
10	damping coefficient g_{22}	3.2
11	proportional coefficient kp	0.12
12	integral coefficient ki	0.25

According to the CPL equivalent circuit, the CPL can be equivalent to the parallel connection of a CCS and a negative resistor. In the simulation, another CCS is used to control the negative resistor's current, which is decided by power and voltage, as shown in Figure 3.

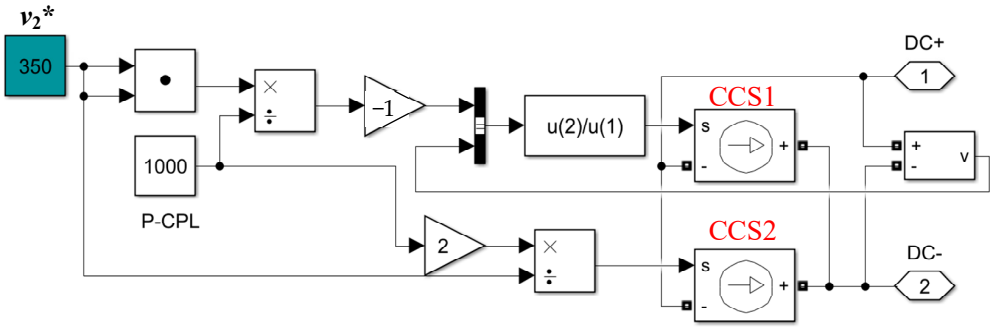

Figure 3. CPL simulation model.

4.1. CPL Perturbation Simulation

Figure 4 shows voltages and power waveforms in the CPL step change simulation. In the simulation, a 750 V source supplies the DAB's primary side, the CPL connects to its secondary side, and the reference v_2* is set as 375 V. At the time t_1, the power is set as 15 kW, then the power is set as −15 kW at the time t_2.

It can be seen that the power tracks the reference value quickly without obvious voltage fluctuations, and it has a smaller ripple voltage compared with PI control. The PBC has a good response characteristic when a CPL perturbation occurs.

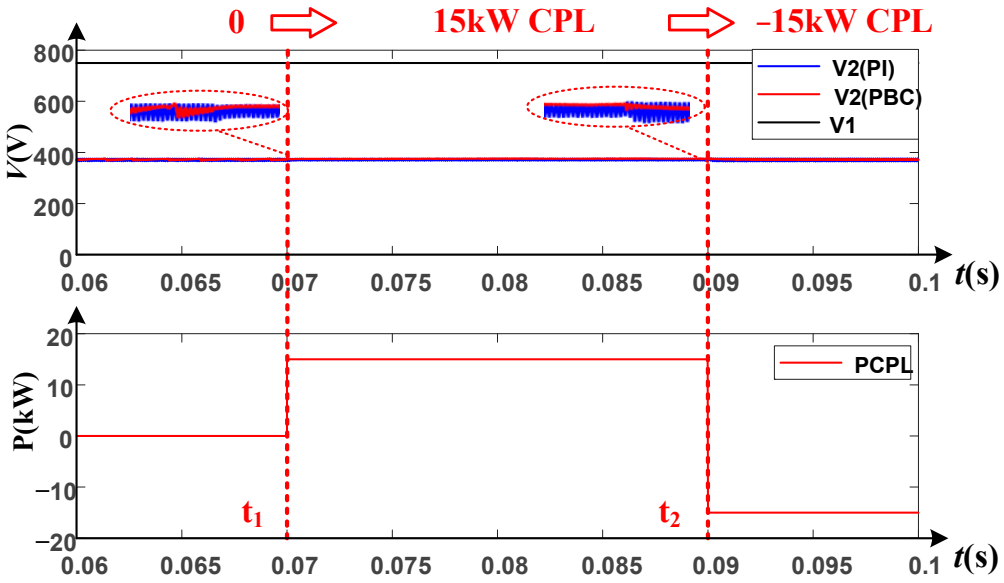

Figure 4. Waveforms in CPL perturbation simulation.

4.2. Source Perturbation Simulation

Figure 5 shows voltages and power waveforms in source perturbation simulation. In the simulation, a controlled voltage source (CVS) supplies the DAB's primary side, the CPL also connects to the DAB's secondary side, and the reference v_2* is also set as 375 V. At the time t_3, the power supply voltage decreases rapidly to 600 V and restores to the normal voltage at the time t_4.

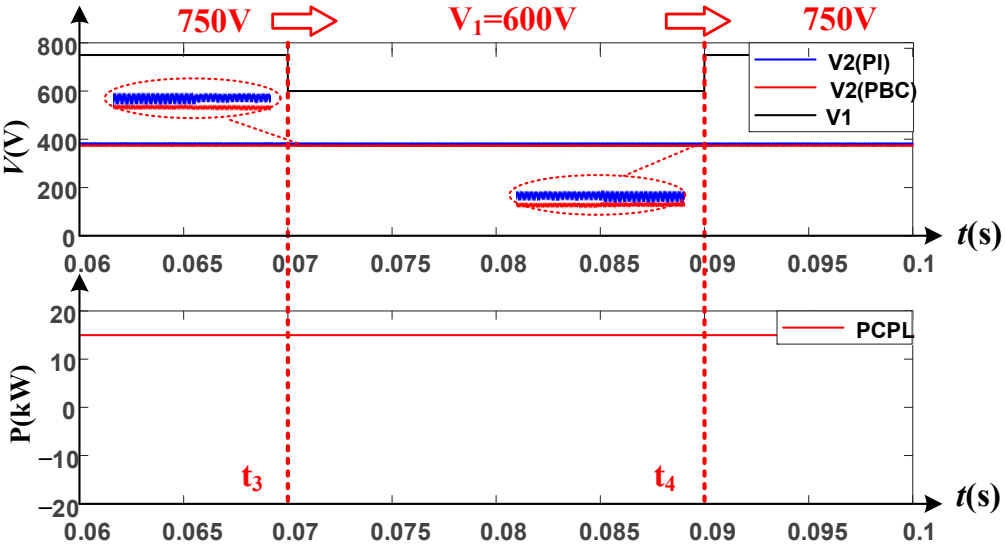

Figure 5. Waveforms in source perturbation simulation.

This shows that the secondary voltage v_2 has no obvious fluctuations during the transient process, and PBC has better response characteristics and smaller voltage ripples compared to PI control when in the source perturbation condition.

4.3. Voltage Reference Step Simulation

Figure 6 shows voltages and power waveforms in reference step change simulation. In the simulation, a power source supplies the DAB's primary side; the CPL connects to the DAB's secondary side. First, the reference v_2* is set as 375 V, and it is set as 300 V at the time t_5; then, it is reset as 375 V again at the time t_6. This shows that the secondary

voltage tracks the reference step with a transient process, and it also has good response characteristics.

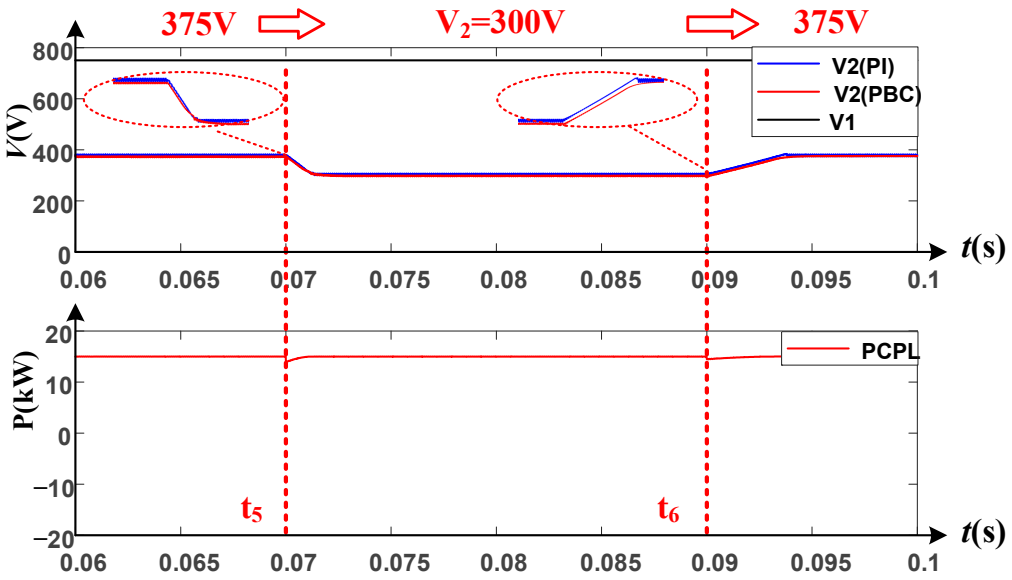

Figure 6. Waveforms in reference step simulation.

Through the simulations, it can be concluded that the proposed PBC control can stabilize secondary voltage without obvious fluctuation, whether in a load or source perturbation condition or in a reference step change condition, and it has better response characteristics than PI control.

5. Experiment

The experimental setup, which is used for the validation of the proposed PBC based on the EL model, is presented in Figure 7, and its main circuit parameters are listed in Table 2. In the experiment, an electronic load APL-II (Myway company) is used to simulate a CPL, and a bidirectional power source PSB9750 (EA company) is used to simulate the power supply. Voltage perturbation, power perturbation, and reference step change experiments are also carried out in the platform.

Table 2. Main parameters of DAB converter prototype.

	Parameters	Value
1	DC voltage v_1 (V)	300
2	capacitance C_1 (μF)	1360
3	resistance R_1 (Ω)	200×10^3
4	voltage v_2 (V)	150
5	capacitance C_2 (μF)	5440
6	resistance R_2 (Ω)	100×10^3
7	inductance L_1 (μH)	156
8	HF transformer's turn ratio	300:150
9	DAB switching frequency (kHz)	20
10	damping coefficient g_{22}	13

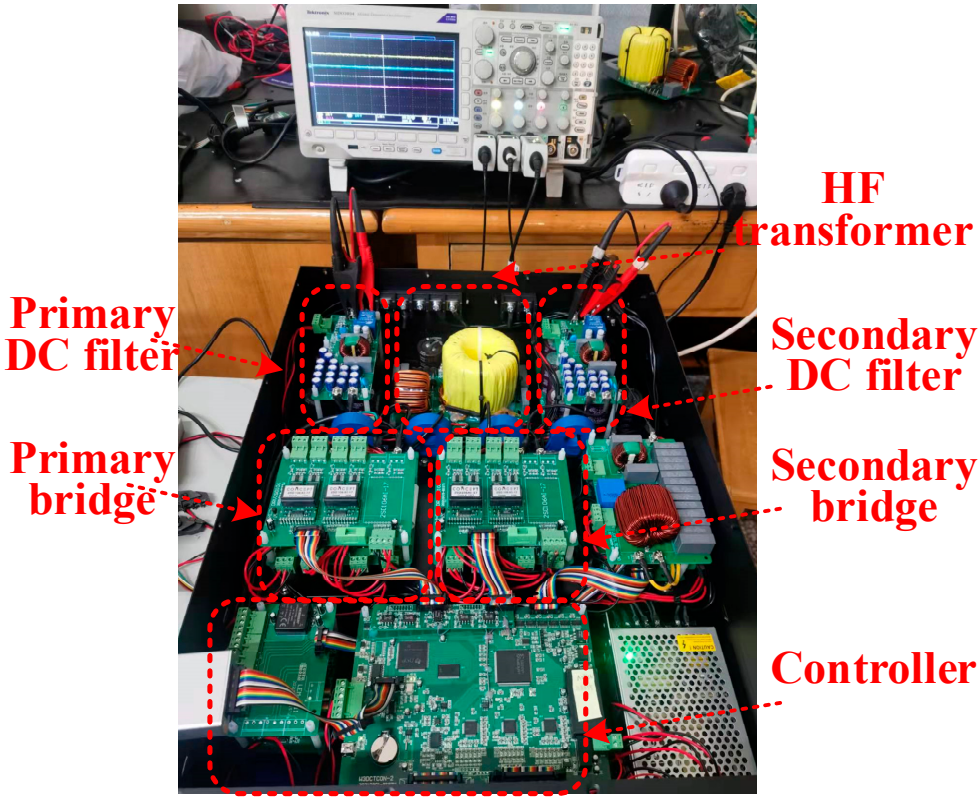

Figure 7. The DAB converter prototype.

5.1. Starting Experiment

Figure 8 gives the voltages and current waveforms of the DAB converter when starting the process. At the time t_1, the DAB converter begins to start in CSV mode, and the secondary voltage increases gradually. At the time t_2, the soft starting process ends, and the PBC control starts. At the time t_3, the secondary voltage is stable at the set value (100 V), and the starting process ends.

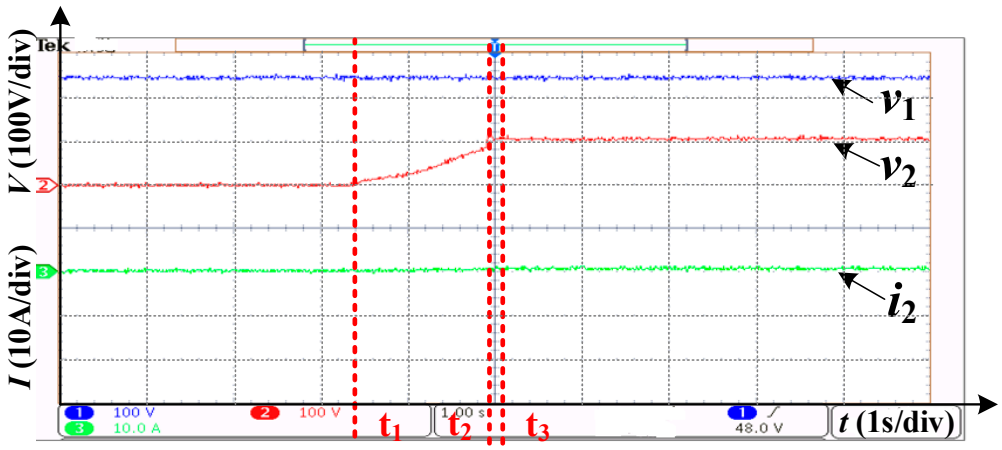

Figure 8. Waveforms in starting experiment.

This shows that the voltage overshot is about 8 V, the whole starting time is 1.6 s, and it has quick starting and low voltage overshoot characteristics.

5.2. CPL Perturbation Experiment

Figure 9 gives the voltages and current waveforms of the DAB converter in the CPL perturbation experiment. In Figure 9a, the secondary voltage is stable at an initial 100 V. At

the time t_4, a 1 kW CPL switches on, and the secondary current increases gradually. At the time t_5, the secondary current is stable at 10 A. At the time t_6, the CPL is cut off, and the secondary current recovers to 0 quickly.

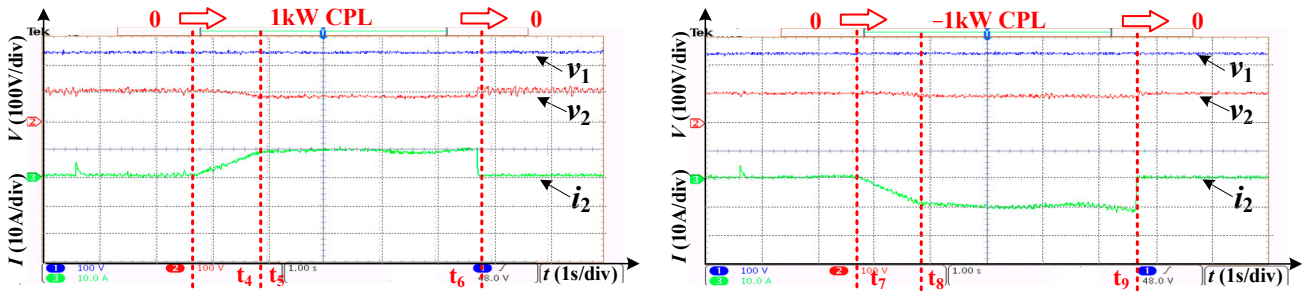

Figure 9. Waveforms in CPL perturbation experiment. (**a**) positive CPL load. (**b**) negative CPL load.

In Figure 9b, the secondary voltage is also stable at an initial 100 V. At the time t_7, a −1 kW CPL switches on, and the secondary current decreases gradually. At the time t_8, the secondary current is stable at −10 A. At the time t_9, the CPL is switched off, and the secondary current also recovers to 0 quickly.

This shows that when a CPL is switched on, the secondary current increases or decreases gradually, and when the CPL is cut off, the secondary current restores to 0 quickly. The secondary voltage has no obvious overshot or sag in the whole dynamic process. This means that the PBC control has a good transient performance.

5.3. Source Perturbation Experiment

Figure 10 gives the voltages and current waveforms of the DAB converter in a source perturbation experiment. At first, the source voltage is 250 V, and the secondary voltage is stable at 80 V with a 1 kW CPL. At the time t_{10}, the source voltage drops to 230 V suddenly, and the secondary voltage remains stable with slight fluctuation. At the time t_{11}, the source voltage restores to 250 V suddenly, and the secondary voltage also remains stable at the same time. This shows that the DAB converter can stabilize the secondary voltage with large source perturbation.

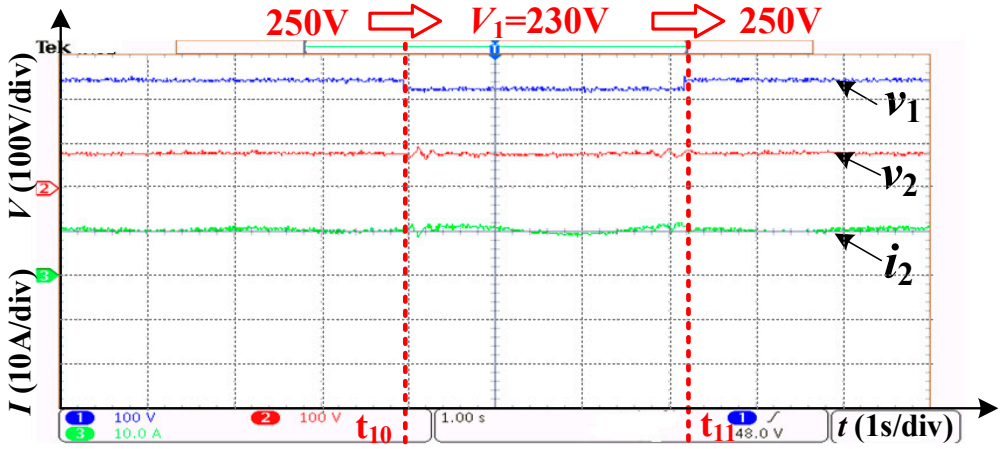

Figure 10. Waveforms in source perturbation experiment.

5.4. Voltage Reference Step Experiment

Figure 11 gives the voltages and current waveforms of the DAB converter in the voltage reference step change experiment. At first, the source voltage is 250 V, and the secondary voltage is stable at 80 V with a 1 kW CPL. At the time t_{12}, the reference voltage

is set to 50 V suddenly, the voltage tracks the reference quickly, and the current increases correspondingly. At the time t_{13}, the reference voltage is reset to 80 V suddenly, the voltage also tracks the reference quickly, and the current also decreases correspondingly. This shows that the DAB converter has a good dynamic response characteristic.

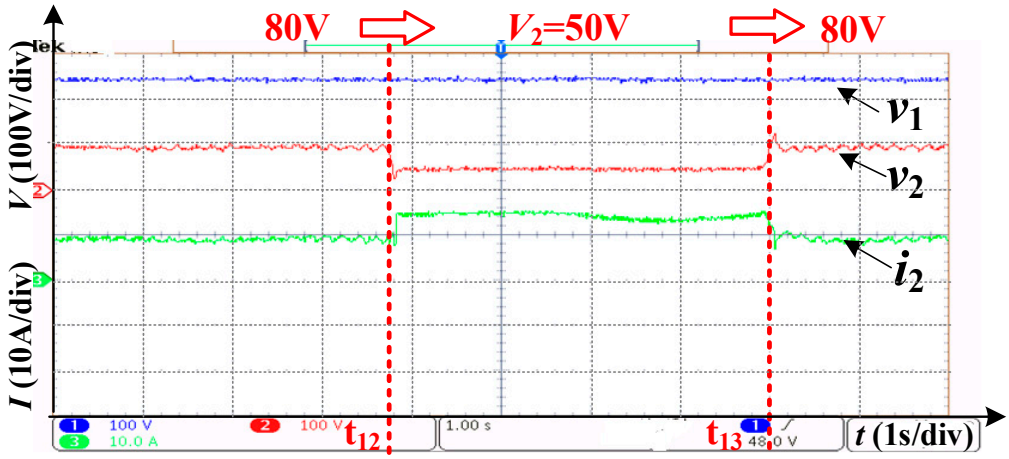

Figure 11. Waveforms in voltage reference step experiment.

6. Conclusions

This paper develops a practical PBC controller based on the EL model for the DAB converter. This controller is validated under different conditions, including source perturbation, CPL perturbation, and reference step change. Compared with the previous approaches, the proposed approach has a definite physical meaning which is deduced from Kirchhoff's law, and it is more suitable for voltage-stabilizing control scenarios. The results, which are obtained from simulations and low-power prototype experiments, prove its feasibility and good performance.

Author Contributions: Data curation, Y.Z. (Yajing Zhang) and J.W.; Funding acquisition, Y.Z. (Yuming Zhao); Investigation, X.W.; Writing—original draft, J.L. All authors have read and agreed to the published version of the manuscript.

Funding: This research was funded by The Beijing Natural Science Foundation Program of China (no. 3202010), Key Science and Technology Projects of China Southern Power Grid Corporation (no. 090000KK52210132) and The National Natural Science Foundation of China (no. 52107176, 52237008).

Conflicts of Interest: The authors declare no conflict of interest.

References

1. Walter, J.; De Doncker, R. High-power galvanically isolated DC/DC converter topology for future automobiles. In Proceedings of the IEEE 34th Annual Conference on Power Electronics Specialist, Acapulco, Mexico, 15–19 June 2003; Volume 1, pp. 27–32.
2. Kheraluwala, M.; De Doncker, R. Single phase unity power factor control for dual active bridge converter. In Proceedings of the IEEE Industry Applications Conference 28th IAS Annual Meeting, Toronto, ON, Canada, 2–8 October 1993; Volume 2, pp. 909–916.
3. De Doncker, R.W.; Divan, D.M.; Kheraluwala, M.H. A three phase soft switched high power density DC/DC converter for high power applications. *IEEE Trans. Indus. Appl.* **1988**, *27*, 63–73. [CrossRef]
4. Zhao, B.; Song, Q.; Liu, W.; Sun, Y. Overview of dual-active-bridge isolated bidirectional dc–dc converter for high-frequency-link power-conversion system. *IEEE Trans. Power Electron.* **2014**, *29*, 4091–4106. [CrossRef]
5. Zhao, B.; Song, Q.; Liu, W.; Sun, Y. Dead-time effect of the high-frequency isolated bidirectional full-bridge dc–dc converter: Comprehensive theoretical analysis and experimental verification. *IEEE Trans. Power Electron.* **2014**, *29*, 1667–1680. [CrossRef]
6. López-Rodríguez, K.; Escobar-Mejía, A.; Piedrahita-Echavarria, E.Y.; Gil-González, W. Passivity-Based Current Control of a Du-al-Active Bridge to Improve the Dynamic Response of a Solid-State Transformer During Power and Voltage Variations. In Proceedings of the IEEE 11th International Symposium on Power Electronics for Distributed Generation Systems (PEDG), Dubrovnik, Croatia, 28 September–1 October 2020; pp. 230–235.
7. Cupelli, M.; Zhu, L.; Monti, A. Why ideal constant power loads are not the worst case condition from a control stand-point. *IEEE Trans. Smart Grid* **2015**, *6*, 2596–2606. [CrossRef]

8. Emadi, A.; Khaligh, A.; Rivetta, C.H.; Williamson, G.A. Constant power loads and negative impedance instability in automotive systems: Definition modelling stability and control of power electronic converters and motor drives. *IEEE Trans. Veh. Technol.* **2006**, *55*, 1112–1125. [CrossRef]
9. Martinez-Lopez, M.; Moreno-Valenzuela, J.; He, W. A robust nonlinear PI-type controller for the DC–DC buck–boost power converter. *ISA Trans.* 2022; *in press*. [CrossRef]
10. Bobtsov, A.; Ortega, R.; Nikolaev, N.; He, W. A globally stable practically implementable PI passivity-based controller for switched power converters. *arXiv* **2020**, arXiv:2005.01671. [CrossRef]
11. Ai, X.; Zuo, D.; Zhang, Y. Modeling and Simulation of Dual-Active-Bridge Based on PI Control. *J. Phys. Conf. Ser.* **2022**, *2221*, 012007. [CrossRef]
12. Qin, H.; Kimball, J.W. Generalized Average Modeling of Dual Active Bridge DC–DC Converter. *IEEE Trans. Power Electron.* **2011**, *27*, 2078–2084. [CrossRef]
13. Li, H.; Peng, F.Z.; Lawler, J.S. A natural zvs medium-power bidirectional dc-dc converter with minimum number of devices. *IEEE Trans. Ind. Appl.* **2003**, *39*, 525–535.
14. Krismer, F.; Kolar, J.W. Closed form solution for minimum conduction loss modulation of dab converters. *IEEE Trans. Power Electron.* **2011**, *27*, 174–188. [CrossRef]
15. Krismer, F.; Kolar, J.W. Accurate small-signal model for the digital control of an automotive bidirectional dual active bridge. *IEEE Trans. Power Electron.* **2009**, *24*, 2756–2768. [CrossRef]
16. Cardozo DD, M.; Balda, J.C.; Trowler, D.; Mantooth, H.A. Novel nonlinear control of dual active bridge using simplified converter model. In Proceedings of the 25th IEEE Annual Applied Power Electronics Conference and Exposition (APEC), Palm Springs, CA, USA, 21–25 February 2010; p. 7.
17. Phattanasak, M.; Gavagsaz-Ghoachani, R.; Martin, J.P.; Pierfederici, S.; Davat, B. Flatness based control of an isolated three-port bidirectional dc-dc converter for a fuel cell hybrid source. In Proceedings of the IEEE Energy Conversion Congress and Exposition (ECCE), Phoenix, AZ, USA, 17–22 September 2011; pp. 977–984.
18. Phattanasak, M.; Gavagsaz-Ghoachani, R.; Martin, J.-P.; Nahid-Mobarakeh, B.; Pierfederici, S.; Davat, B. Comparison of two nonlinear control strategies for a hybrid source system using an isolated three-port bidirectional DC-DC converter. In Proceedings of the 2011 IEEE Vehicle Power and Propulsion Conference, Chicago, IL, USA, 6–9 September 2011; pp. 1–6.
19. Zhang, H.; Li, Y.; Li, Z.; Zhao, C.; Gao, F.; Hu, Y.; Luo, L.; Luan, K.; Wang, P. Model predictive control of input-series output-parallel dual active bridge converters based DC transformer. *IET Power Electron.* **2020**, *13*, 1144–1152. [CrossRef]
20. Xiao, Z.; Lei, W.; Gao, G.; Cui, Y.; Kang, Q.; Wang, M. Transient Current Constraint of DAB Converter Based on Model Predictive Control. In Proceedings of the 2020 IEEE 9th International Power Electronics and Motion Control Conference (IPEMC2020-ECCE Asia), Nanjing, China, 29 November–2 December 2020; pp. 203–207.
21. Jeung, Y.-C.; Lee, D.-C. Voltage and current regulations of bidirectional isolated dual-active-bridge DC–DC converters based on a double-integral sliding mode control. *IEEE Trans. Power Electron.* **2019**, *34*, 6937–6946. [CrossRef]
22. Li, K.; Yang, Y.; Tan, S.-C.; Hui, R.S.-Y. Sliding-Mode-Based Direct Power Control of Dual-Active-Bridge DC-DC Converters. In Proceedings of the 2019 IEEE Applied Power Electronics Conference and Exposition (APEC), Anaheim, CA, USA, 17–21 March 2019; pp. 188–192.
23. Song, W.; Hou, N.; Wu, M. Virtual Direct Power Control Scheme of Dual Active Bridge DC–DC Converters for Fast Dynamic Response. *IEEE Trans. Power Electron.* **2018**, *33*, 1750–1759. [CrossRef]
24. Xu, Q.; Vafamand, N.; Chen, L.; Dragicevic, T.; Xie, L.; Blaabjerg, F. Review on Advanced Control Technologies for Bidirectional DC/DC Converters in DC Microgrids. *IEEE J. Emerg. Sel. Top. Power Electron.* **2020**, *9*, 1205–1221. [CrossRef]
25. Ortega, R.; van der Schaft, A.; Maschke, B.; Escobar, G. Interconnection and damping assignment passivity-based control of port-controlled Hamiltonian systems. *Automatica* **2002**, *38*, 585–596. [CrossRef]
26. Li, J.; Lv, X.; Zhao, B.; Zhang, Y.; Zhang, Q.; Wang, J. Research on Passivity Based Control Strategy of Power Conversion System used in the Ener-gy Storage System. *IET Power Electron.* **2019**, *12*, 392–399. [CrossRef]
27. Li, J.; Wang, M.; Zhao, Y.; Wang, J.; Yang, D.; Lv, X. Passivity-based control of the hybrid rectifier for medium and high-power application. *IET Power Electron.* **2019**, *12*, 4070–4078. [CrossRef]
28. Yuanpeng FE, N.G.; Jiuhe WA, N.G.; Jianguo, L.I. Control strategy of Vienna rectifier with LCL filter under weak grid conditions. *Power Gener. Technol.* **2019**, *40*, 286–293.
29. Biel, D.; Scherpen, J.M.A. Passivity-based control of active and reactive power in single-phase PV inverters. In Proceedings of the 2017 IEEE 26th International Symposium on Industrial Electronics (ISIE), Edinburgh, UK, 19–21 June 2017.
30. Liu, G.; Wang, W.; Wang, W.; Zhu, K. Power Feedforward Method for Passivity-based Grid-connected PV Inverter in Weak Grids. In Proceedings of the 2018 IEEE 4th Southern Power Electronics Conference (SPEC), Singapore, 10–13 December 2018; pp. 1–6.
31. Gui, Y.; Kim, W.; Chung, C.C. Passivity-Based Control With Nonlinear Damping for Type 2 STATCOM Systems. *IEEE Trans. Power Syst.* **2016**, *31*, 2824–2833. [CrossRef]
32. Jiang, Y.; Qin, C.; Xing, X.; Li, X.; Zhang, C. A Hybrid Passivity-Based Control Strategy for Three-Level T-Type Inverter in LVRT Operation. *IEEE J. Emerg. Sel. Top. Power Electron.* **2019**, *8*, 4009–4024. [CrossRef]
33. Zhao, J.; Wu, W.; Gao, N.; Wang, H.; Chung, H.; Blaabjerg, F. Combining Passivity-Based Control with Active Damping to Improve Stability of LCL Filtered Grid-Connected Voltage Source Inverter. In Proceedings of the 2018 IEEE International Power Electronics and Application Conference and Exposition (PEAC), Shenzhen, China, 4–7 November 2018; pp. 1–6.

34. Meshram, R.V.; Bhagwat, M.; Khade, S.; Wagh, S.R.; Stankovic, A.M.; Singh, N.M. Port-Controlled Phasor Hamiltonian Modeling and IDAPBC Control of Solid-State Transformer. *IEEE Trans. Control Syst. Technol.* **2017**, *27*, 161–174. [CrossRef]
35. Cupelli, M.; Gurumurthy, S.K.; Bhanderi, S.K.; Yang, Z.; Joebges, P.; Monti, A.; De Doncker, R.W. Port Controlled Hamiltonian Modeling and IDA-PBC Control of Dual Active Bridge Converters for DC Microgrids. *IEEE Trans. Ind. Electron.* **2019**, *66*, 9065–9075. [CrossRef]
36. Cupelli, M.; Bhanderi, S.K.; Gurumurthy, S.K.; Monti, A. Port—Hamiltonian Modelling and Control of Single Phase DAB Based MVDC Shipboard Power System. In Proceedings of the IECON 2018—44th Annual Conference of the IEEE Industrial Electronics Society, Washington, DC, USA, 21–23 October 2018; pp. 3437–3444.